Synthesis and Phase Structures of Mesogen-Jacketed Liquid Crystalline Polymers Containing 1,3,4-Oxadiazole Based Side Chains

Chun-Peng Chai,[†,‡] Xing-Qi Zhu,[†] Ping Wang,[†] Min-Qiao Ren,[†] Xiao-Fang Chen,[†] Yi-Ding Xu,[†] Xing-He Fan,*[,†] Chun Ye,[†] Er-Qiang Chen,*[,†] and Qi-Feng Zhou*[,†]

Beijing National Laboratory for Molecular Sciences, Key Laboratory of Polymer Chemistry and Physics of Ministry of Education, College of Chemistry and Molecular Engineering, Peking University, Beijing 100871, China, and School of Materials Science & Engineering, Beijing Institute of Technology, Beijing 100081, China

Received July 26, 2007; Revised Manuscript Received October 28, 2007

ABSTRACT: A series of new monomers of 2,5-bis[(4-tertbutyl-phenyl)-1,3,4-oxadiazole] styrene (M-Ct) and 2,5-bis[(4-alkoxy-phenyl)-1,3,4-oxadiazole]styrene (M−OC*m*, *m* is the number of the carbons in the alkoxy groups, $m = 8, 10, 12, 14$) were synthesized. Conventional radical polymerization of the monomers resulted in a series of new mesogen-jacketed liquid crystalline polymer (MJLCP) containing the 1,3,4-oxadiazole unit. The chemical structures of the monomers were confirmed by elemental analysis, mass spectrometry, ^{1}H NMR, and IR. The molecular characterization of the corresponding polymers of P-Ct and P-OC*m*s was performed with ^{1}H NMR, gel permeation chromatography, and thermogravimetric analysis. Their phase structures and transitions were investigated by differential scanning calorimetry, wide-angle X-ray diffraction, and polarized light microscopy experiments. The P-Ct formed the hexatic columnar nematic (Φ_{HN}) phase that is typical for MJLCPs, wherein the chain molecules were rodlike. The P-OC*m*s exhibited a well-defined smectic A (S_A) phase. As the mesogenic group is laterally jacketed to the polyethylene backbone through a single carbon−carbon bond, the P-OC*m* molecule in the S_A phase should be more or less ribbonlike with the backbone squeezed by the parallel aligned side chains on both sides. The transition of the four P-OC*m*s follows the sequence of $S_A \leftrightarrow N \leftrightarrow I$. The comparison between P-Ct and P-OC*m*s indicates that the flexibility of the side-chain tails is crucial to determine the LC structures. Namely, simply changing the chemical structures of small portion of the MJLCP may greatly vary the molecular packing behavior and thus the molecular shape in LC phase structures.

Introduction

Liquid crystalline (LC) polymers have received long-standing attention for the fundamental research on their phase structures and transitions and for their applications in engineering plastics, optoelectronic or nonlinear optic devices, light-emitting materials, etc. The mesogenic groups incorporated in the side-chain LC polymers can be linked to the backbone via either "terminal" or "lateral" attachment.[1,2] In order to decouple the dynamics of side chains and backbones, flexible spacers with reasonable length are usually introduced.[3,4] Consequently, the LC properties of side-chain LC polymers are highly dependent on the mesogenic groups, and the low-ordered LC phases, such as nematic (N), smectic A (S_A), and smecitic C (S_C) phases, can be readily formed. When flexible spacers are absent, the phase structures and transitions of the side-chain LC polymers may become very different. In 1987, Zhou et al. have reported the first example of a mesogen-jacketed LC polymer (MJLCP).[5] The chemical feature of the MJCPL is that the "waist" of the side-chain mesogenic group is laterally attached to the every second carbon atom along the backbone without a spacer or with a very short linkage.[5−11] In this case, a strong steric interaction between polymer backbones and bulky side chains is introduced. The polymer backbones are thus forced to adopt a more extended conformation to accommodate bulky side chains, which has been evidenced by small-angle neutron scattering (SANS).[12,13] In solutions, the MJLCP can possess relatively long persistence lengths, demonstrating a behavior similar to rigid polymer chains.[14]

In many MJLCPs with the side chains linked to the backbone through a single carbon−carbon bond, wide-angle X-ray diffraction (WAXD) and polarized light microscopy (PLM) experiments have revealed that their behavior is no longer determined by the mesogenic groups. Unlike conventional side-chain LC polymers that form nematic or smectic phases, MJLCPs can pack into columnar LC (Φ) phases including columnar nematic (Φ_H) and hexatic columnar nematic (Φ_{HN}) phases.[15−17] The building blocks of Φ phases of MJLCPs are molecular rods, which can be constructed by wrapping bulky side chains around the somewhat extended backbones. The molecular weight (MW), on which the rod length depends, should be large enough to stabilize the LC phases.[15,18] It has been found that laterally jacketing nonmesogenic side chains to polymer backbones can also lead to the molecular rods in the bulk state.[19,20] Once the relatively flexible side chains with a certain size can impose sufficient steric hindrance to the polyethylene backbone, a long-range ordered hexagonal columnar (Φ_H) phase can be achieved.[20] This behavior can be analogous to that observed in monodenron-jacketed polymers[21−23] and other flexible side-chain polymers[24,25] possessing columnar mesophase. Moreover, MJLCPs can serve as "rods" to form rod−coil block copolymers.[26−32] Within the microphase separated ordered structures, the MJLCP rods pack parallel to form Φ phases.[31,32]

However, the rodlike chain shall not be the only molecular shape of MJLCPs. S_A and S_C phases have been found in laterally attached side-chain LC polymers.[33−39] For example, Komp and Finkelmann has recently reported that a macroscopically oriented S_A LC elastomer can be composed of a poly(methylsiloxane) backbone and side-on attached mesogenic units with reasonably long spacers.[33] Particularly, the laterally attached side-chain LC

* To whom the correspondence should be addressed. E-mail: fanxh@pku.edu.cn (X.-H.F.); eqchen@pku.edu.cn; qfzhou@pku.edu.cn (E.-Q.C.).
† Peking University.
‡ Beijing Institute of Technology.

10.1021/ma071670t CCC: $37.00
Published on Web 11/29/2007

Scheme 1. Synthetic Route of the Monomers and Polymers

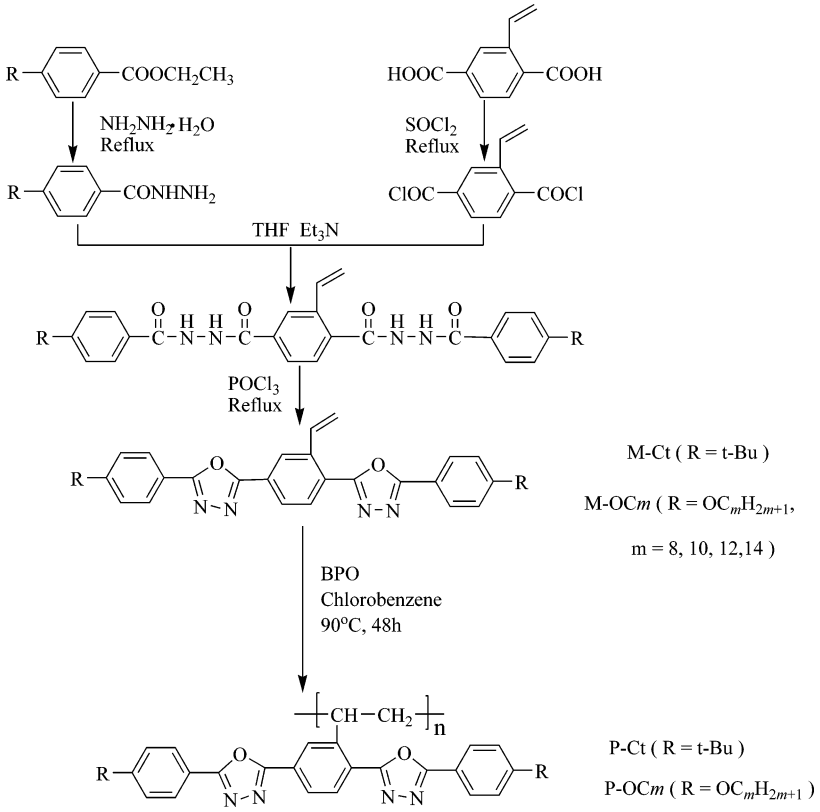

polynorbornene with a one-carbon spacer exhibits a stable S_C phase and can undergo a second-order S_C-to-S_A transition upon heating.[38] Recently, we have synthesized two new MJLCPs, poly[4,4′-bis(4-butoxyphenyloxycarbonyl)-2-vinylbiphenyl] (PBP-2VBP) and poly[4,4′-bis(4-butoxyphenyloxycarbonyl)-3-vinylbiphenyl] (PBP3VBP), and their LC phases of S_A were identified.[40] Compared with other MJLCPs we previously studied, such as poly{2,5-bis [(4-methoxyphenyl)oxycarbony]-styrene} (PMPCS), the PBP2VBP and PBP2VBP possess a larger aspect ratio, which might be one of the reasons for the formation of the S_A phase. It is suggested that the PBP2VBP and PBP3VBP molecules in their S_A phases are more ribbonlike rather than rodlike.

To explore their potential, we are currently interested in functionalization of the MJLCPs. We first intended to design a MJLCP with a laterally attached mesogen containing the 1,3,4-oxadiazole group. It is well-known that 2,5-diaryl-1,3,4-oxadiazole (OXD) derivatives demonstrate high photoluminescence quantum yields and good thermal and chemical stabilities.[41] Such properties, combined with the electron-deficient nature of the oxadiazole ring, can lead to the applications as electron-transporting/hole-blocking materials in organic light-emitting devices (OLEDs).[42,43] The low-molecular weight compounds,[44−46] dendritic,[47] and polymeric derivatives[48−51] containing OXDs have been studied. We aimed to incorporate the OXD groups into a new series of MJLCPs. The chemical structure of the polymer we designed and synthesized is as follows:

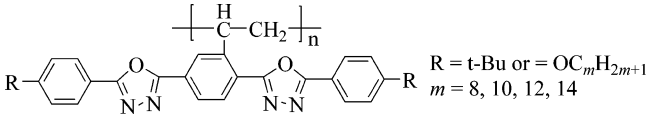

In this paper, we describe the synthesis of the monomers and the polymers and the LC phase structures and transitions of the polymers as well. Our experimental results confirm again that the monomer containing a large mesogenic substitute on one of the vinyl carbons can be easily polymerized by the radical polymerization method. Interestingly, the resultant polymers can form not only the Φ phase but also the S_A phase, of which the phase structures are strongly dependent on the chemical structure of the end groups on the side chains. Namely, the polymer with the *tert*-butyl end groups (P-Ct) can develop into a Φ_{HN} phase. On the other hand, with the relatively long *n*-alkoxy substituents as the tail, the polymers (P-OC*m*, $m = 8, 10, 12, 14$) have demonstrated a well-defined S_A phase having the layer period determined by the side-chain lengths at low temperature. The S_A formation of P-OC*m* may be attributed to that the flexible *n*-alkoxy tails enhance the mobility of the OXD-based side chains, resulting in the parallel packing of the mesogenic groups. While P-Ct possesses the Φ_{HN} phase stable in the entire temperature range we studied, the phase transition sequence of P-OC*m*s is $S_A \leftrightarrow N \leftrightarrow$ Isotropic (I).

Experimental Section

Materials. The compound of vinylterephthalic acid was synthesized using the method previously reported.[9] Benzoyl peroxide (BPO) was purified by recrystallization from ethanol. Chlorobenzene was washed with H_2SO_4, $NaHCO_3$, and distilled water separately and was distilled from calcium hydride. THF (AR; Beijing Chemical Co.) and pyridine (Acros, 99%) were heated under reflux over calcium hydride for at least 8 h and distilled before use. All other reagents were used as received from commercial sources.

Synthesis of Monomers. The synthetic route of the monomers of 2,5-bis[(4-tertbutyl-phenyl)-1,3,4-oxadiazole]styrene (M-Ct) and 2,5-bis[(4-alkoxy-phenyl)-1,3,4-oxadiazole]styrene (M-OC*m*, *m* is the number of the carbons in the alkoxy groups, $m = 8, 10, 12, 14$) is shown in Scheme 1. The experimental details of the monomer synthesis and characterization are described below using M-Ct as an example. The mass spectrometry and elemental analysis data of the monomers are provided in the Supporting Information.

(a) Synthesis of *p-tert*-Butyl-benzhyhydrazide. In a 250 mL round-bottom flask attached with a reflux condenser, *p-tert*-butyl-ethyl-benzoate (20.6 g, 10 mmol) was dissolved in 100 mL of ethanol, and 40 mL of hydrazinium hydrate was added at room temperature with stirring. The reaction mixture was boiled gently for 14 h, resulting in a colorless transparent solution. After the mixture was cooled to room temperature, most of the solvent was removed by evaporation under reduced pressure and 200 mL of water was then added. The solid product in the mixture was obtained by filtration and was washed with dilute HCl, saturated sodium bicarbonate, and water. After drying, the product was further washed several times with petroleum ether. The final product of *p-tert*-butyl-benzhyhydrazide was white powder with a yield of 16.3 g (85%). Elemental analysis found (calcd): C%, 68.93 (68.72); H%, 8.27 (8.39); N%, 14.50 (14.57).

(b) Synthesis of Vinylterephthal Chloride. An amount of 1.92 g (10 mmol) of vinylterephthalic acid was mixed with thionyl chloride in a 100 mL round-bottom flask. The mixture was refluxed for about 2 h to give a clear solution. The excess thionyl chloride was removed by evaporation under reduced pressure. The residue was washed twice by petroleum ether. A pale yellow liquid of vinylterephthal chloride was obtained with a yield of 95%. ^{1}H NMR [$CDCl_3$] (δ): 8.38, 8.26, 8.19 (m, 3H, −Ar−H), 7.25 (m, 1H, −CH═), 6.06, 5.49 (d, 2H, ═CH_2).

(c) Synthesis of Bishydrazide. 3.85 g (20 mmol) of *p-tert*-butyl-benzhyhydrazide, 0.03 g of 2,6-diterbutyl-*p*-methoxyphenol, and 10 mL of triethylamine were dissolved in 60 mL of dried THF. An amount of 2.29 g (10 mmol) of vinylterephthal chloride was dissolved in 20 mL of dried THF. Under intense stirring at the temperature of the ice bath, the solution of vinylterephthal chloride was slowly dropped into the solution of *p-tert*-butyl-benzhyhydrazide over a 2 h time period. A vigorous reaction occurred, leading to a white suspension. When the mixture became too viscous, THF was added as a diluter (total of 10 mL). The mixture was further stirred at room temperature for 14 h, and then most of the THF was distilled off the system by evaporation under reduced pressure. After water was added into the residue, the crude solid product of bishydrazide was collected by filtration. To remove reagents, the product was washed sequentially with dilute HCl, water, saturated sodium bicarbonate, water, and THF three times. No further purification was conducted because the product hardly dissolved in any common organic solvent.

(d) Synthesis of 2,5-Bis[(5-*tert*-butyl-phenyl)-1,3,4-oxadiazole]-styrene (M-Ct). A mixture of 3.5 g of bishydrazide, 30 mL of phosphorus oxychloride, and 0.03 g of 2,6-diterbutyl-*p*-methoxyphenol in a 100 mL round-bottom flask was refluxed at 110 °C for 14 h and then cooled to room temperature. The reaction mixture was poured slowly into excess ice water with intense stirring, and the product was precipitated out. After the product was washed to neutrality with sodium hydroxide solution, the precipitate was filtered under suction and then dried at ambient conditions. Afterward, the raw product dissolved in dichloroethane was purified first by column chromatography (silica gel, dichloroethane/ethyl acetate, 8/1), followed by recrystallization from THF to yield 2.38 g of M-Ct (68%). IR (cm^{-1}): 3075, 3043 (ν_{Ar-H}, $\nu_{C=CH}$); 2955, 2873 ($\nu_{-CH2,\ -CH3}$); 1609, 1560, 1498, 1476 (phenyl $\nu_{C=C}$), 1347-($\nu_{C=N}$); 1303, 1257, 1175 (ν_{C-O-C}). ^{1}H NMR (δ): 1.39 (s, 18H, −CH_3), 5.62, 5.99 (d, 2H, ═CH_2), 7.93 (m, 1H, −CH═), 8.16, 8.08, 7.04 (m, 10H, Ar−H), 8.43 (s, 1H, Ar−H). MS (*m*/*z*): 504. Elemental analysis found (calcd): C%, 76.02 (76.16); H%, 6.53 (6.39); N%, 10.99 (11.10).

Polymerization. All polymers (denoted as P-Ct and P-OC*m* in Scheme 1) were obtained by conventional solution radical polymerization (see Scheme 1). A typical polymerization procedure was carried out as the following. For example, about 0.5 g (1 mmol) of M-Ct, 100 μL of chlorobenzene solution of 0.05 M BPO, and 2 mL of chlorobenzene were transferred into a polymerization tube. After three freeze−pump−thaw cycles, the tube was sealed off under vacuum. Polymerization was carried out at 90 °C for 48 h. The tube was then opened, and the reaction mixture was diluted with 10 mL of THF. The resultant polymer was precipitated and washed with methanol. To completely eliminate the unreacted monomers, the precipitate was redissolved in THF and then reprecipitated in methanol three times. After purification, the polymers were dried to a constant weight.

Instruments and Measurements. ^{1}H NMR (400 MHz) spectra were recorded on a Bruker ARX400 spectrometer at room temperature using deuterated chloroform ($CDCl_3$) as the solvent and tetramethylsilane (TMS) as the internal standard. Elemental analysis was performed with an Elementar Vario EL instrument. Mass spectra were recorded on a Finnigan-MAT ZAB-HS spectrometer. Gel permeation chromatographic (GPC) measurements were carried out at 35 °C on a Waters 2410 instrument equipped with three Waters μ-Styragel columns (10^3, 10^4, and 10^5 Å) in series, using THF as the eluent at a flow rate of 1.0 mL/min. All the GPC data were calibrated with polystyrene standards. The thermogravimetric analysis (TGA) was performed with a TA SDT 2960 instrument at a heating rate of 10 °C/min in a nitrogen or air atmosphere.

Differential scanning calorimetry (DSC, Perkin-Elmer Pyris I with a mechanical refrigerator) was utilized to study the phase transitions of the monomers and the polymers. A typical DSC sample size was ∼5 mg. The samples were encapsulated in hermetically sealed aluminum pans, and the pan weights were kept constant. The temperature and heat flow scale at different cooling and heating rates were calibrated using standard materials such as indium and benzoic acid.

The phase structure evolution of the samples with changing temperature were examined by wide-angle X-ray diffraction (WAXD) powder experiments by using a Philips X'Pert Pro diffractometer with an X'celerator detector in the reflection mode and a Bruker D8Discover diffractometer with GADDS as a 2D detector in the transmission mode. The sample temperature was controlled within ±1 °C. For both diffractometers, the X-ray sources (Cu Kα) were provided by 3 kW ceramic tubes, and the diffraction peak positions were calibrated with silicon powder ($2\theta > 15°$) and silver behenate ($2\theta < 10°$). The sample stage of Philips X'Pert Pro is set horizontally, and the samples were protected by nitrogen purge gas during the measurements. When powder diffractions were recorded by the Bruker D8Discover, the film samples having a thickness of 0.1 mm were sealed between two aluminum foils. To further identify the LC phase structures, the oriented samples were prepared by mechanically shearing from the LC phase when applicable, and the two-dimensional (2D) fiber WAXD were performed with the Bruker D8Discover. The point-focused X-ray beam was aligned either perpendicular or parallel to the mechanical shearing direction. For both the powder one-dimensional (1D) and 2D diffractions, the background scattering was recorded and subtracted from the sample patterns.

To observe the LC textures of the samples, polarized light microscopy (PLM) experiments were carried out on a Leitz Laborlux 12 microscope with a Leitz 350 hot stage. The PLM samples were obtained using small amounts of the polymers which were melt-pressed between two cover glasses.

Results and Discussion

Synthesis and Characterization of the Monomers and Polymers. As shown in Scheme 1, the monomers were synthesized in three steps: (1) synthesis of the *p-tert*-butyl-benzhyhydrazide and vinylterephthal chloride; (2) synthesis of the bishydrazide as a precursor of heterodiazoles,[52,53] and (3) cyclization of the bishydrazide to form the oxadiazole (monomers). In step 2, the obtained bishydrazide could not be dissolved in any common organic solvent and was not purified after reaction. However, in the presence of phosphorus oxychloride, cyclization of the bishydrazide readily occurred at 110 °C. In this case, we used 2,6-diterbutyl-*p*-methoxyphenol to prevent the thermal polymerization of the vinyl groups in the bishydrazide and the resultant monomer. The structures of the monomers have been confirmed by the conventional analysis including ^{1}H NMR, IR, elemental analysis, and mass spectrom-

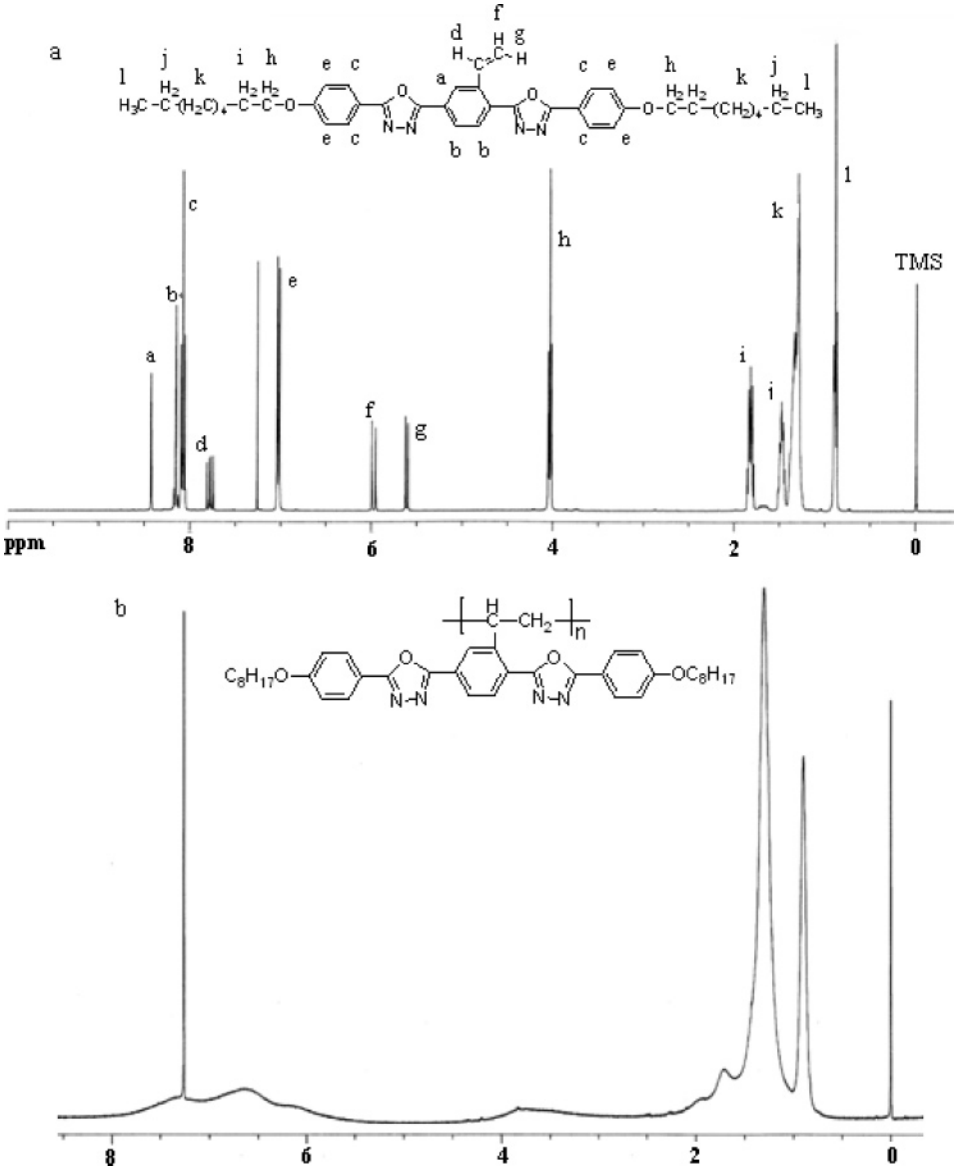

Figure 1. ^{1}H NMR spectra of (a) the monomer M-OC8 and (b) the polymer P-OC8 in $CDCl_3$.

etry (The mass spectrometry and elemental analysis data are provided in Table S1 of the Supporting Information). For the monomers of M-OC*m*, the IR and ^{1}H NMR results were similar to that of the M-Ct shown above.

All the monomers were easily polymerized via the conventional radical polymerization method. Parts a and b of Figure 1 give the ^{1}H NMR spectra of the monomer M-OC8 and the polymer P-OC8, respectively. The M-OC8 shows the characteristic resonances of the vinyl group at 5.4−6.1 and 7.6−7.9 ppm. After polymerization, these signals disappeared completely. The adsorption peaks of P-OC8 are quite broad and consistent with the expected polymer structure. The P-Ct and P-OC*m* were completely soluble in the common organic solvents such as chloroform, THF, chlorobenzene, 1,2-dichlorobenzene, etc. The molecular characterizations of the polymers are summarized in Table 1. The apparent number-average MWs (M_ns) of the polymers by GPC are higher than 1×10^5 g/mol, demonstrating again that the large mesogenic substitute on one of the vinyl carbons does not eliminate the polymerizability of the monomers. The IR and ^{1}H NMR data of the five polymers are summarized in Table S2 of the Supporting Information.

The thermal stability studied by TGA shows that all the polymers are rather stable under nitrogen, of which the temperatures at 5.0% weight loss (T_d) exceed 380 °C (see Table 1). The thermal decomposition of the polymers occurred earlier when the atmosphere changed from nitrogen to air. Compared to the P-Ct with a T_d of 354 °C in air, the P-OC*m*s have much lower T_d's which may be due to the breaking of the ether linkage between the benzene ring and the alkyl tails. As the TGA results showed that the thermal decomposition of the P-OC*m* could initiate at a temperature around 220 °C in air, we performed the experiments with a protection of nitrogen or with the samples sealed between two aluminum foils when the WAXD experiments were carried out.

Table 1. Molecular Characteristics of Polymers

sample	$M_n \times 10^{-4}$ [a]	dw [a]	$T_d(N_2)$ (°C)[b]	T_d(air) (°C)[b]	T_g (°C)
P-Ct	16.0	1.45	394	354	223
P-OC8	12.2	1.42	389	219	148
P-OC10	23.6	1.26	388	216	152
P-OC12	14.2	1.37	387	218	149
P-OC14	10.9	1.57	381	220	148

[a] The apparent number-average molecular weight (M_n) and polydispersity (dw) were measured by GPC using PS standards. [b] The temperatures at 5% weight loss of the samples under nitrogen [$T_d(N_2)$] and in air [T_d(air)] were measured by TGA heating experiments at a rate of 10 °C/min.

Phase Transitions and Phase Structures. All the monomers of M-Ct and M-OC*m* are crystalline at low temperature. Upon

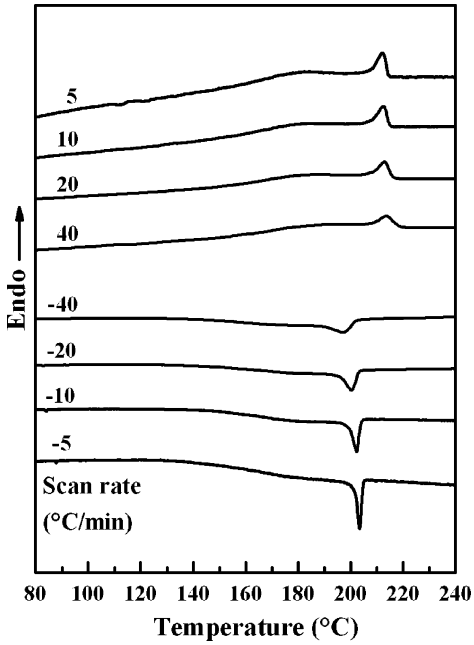

Figure 2. Set of DSC thermal diagrams of P-OC10 at different cooling and heating rates (5−40 °C/min).

heating, M-Ct was melted at 195 °C, immediately followed by a thermal polymerization. For M-OC*m*s, a S_A phase would come after the crystal melting. As evidenced by the WAXD experiments, M-OC*m*s in the S_A phase gave diffractions up to at least the third order, wherein the first-order diffraction corresponded to a *d* spacing identical to the molecular length and the scattering vector ratio of the diffractions followed 1:2:3. Moreover, needle grain textures of M-OC*m*s were observed under PLM. The transition temperatures of S_A to the isotropic state (T_i) decreased with increasing length of the alkoxy tails. For example, the T_i's are 178 and 168 °C for M-OC8 and M-OC14, respectively. M-OC*m*s were also readily thermal polymerized when entering the isotropic state.

The P-Ct and P-OC*m*s obtained by solution radical polymerization are atactic. The DSC cooling and heating experiments found that all the four P-OC*m*s exhibited similar thermal transitions. As an example, Figure 2 shows a set of DSC cooling and subsequent heating thermal diagrams of P-OC10 at different rates (5−40 °C/min). The first-order transition is clear from the exothermic (in cooling) or endothermic (in heating) events. The onset temperature of the higher exothermic peak depends little on the cooling rate, indicating the transition involves a LC phase. In the temperature region below the major peak, a broad transition that looks like only a glass transition is observed. However, careful examination of the DSC baselines indicates that this lower temperature transition is a glass transition overlapped with a broad and weak peak. To separate them well, we annealed the P-OC*m*s samples at 120 °C for 3 h after their thermal history was erased by cooling from the isotropic state. Figure 3 presents the DSC heating diagrams of P-OC*m*s after 120 °C annealing, wherein the glass transition and two endothermic events are obvious. The glass transition temperatures (T_g) of P-OC*m*s, which are defined by the temperature at which 50% devitrification takes place, are listed in Table 1. It is worth noticing that the four P-OC*m*s possess similar T_g's at 150 °C, almost independent of the alkoxy tail length (for the discussion, see below). This glass transition behavior is different from that usually observed in side-chain LC polymers.

The thermal behavior of P-Ct is very different from that of P-OC*m*s but similar to that of other MJLCPs with Φ_N or Φ_{NH}

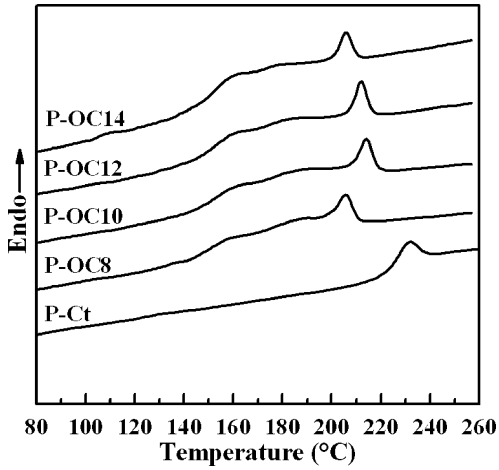

Figure 3. Set of DSC second heating diagrams of P-Ct and P−OC*m*s at a rate of 40 °C/min. Before heating, P-OC*m*s were annealed at 120 °C for 3 h.

we studied before.[15−17] Namely, only the glass transition is observed upon cooling and heating, but no latent heat (i.e., no first-order transition) can be detected by DSC (see Figure 3). Compared to that of P-OC*m*s, the T_g of P-Ct is nearly 70 °C higher. This indicates that when the tail group is changed from flexible alkoxy to rigid *tert*-butyl, the mobility of the polymers is greatly depressed. This will lead to the different LC phase structures for the P-Ct and P-OC*m*s (see below).

To elucidate the phase structures and transitions clearly, we performed WAXD experiments. For both P-Ct and P-OC*m*s, the 1D WAXD patterns in the high 2θ region of 10−30° only rendered an amorphous halo during heating and cooling (see Figure 4), corresponding to the lack of long-range order in the subnanometer length scale. However, at the low 2θ, P-Ct and P-OC*m*s exhibited different diffraction features. Parts a and b of Figure 4 show two sets of 1D WAXD patterns of the P-Ct sample obtained during the first heating and the subsequent cooling, respectively. The sample as-cast from THF solution was amorphous due to the fast solvent evaporation that froze the chain motion toward the ordered structure. In Figure 4a, the low-angle scattering halo at 2θ of 3.5−5.5° is observed below 240 °C; afterward, a diffraction peak gradually develops at the right side of the scattering halo, of which the intensity increases and the peak position slightly shifts toward a lower angle upon heating. At 290 °C, the diffraction peak position is at the $2\theta = 4.73°$ with a *d* spacing of 1.85 nm. Figure 4b shows that this low-angle diffraction evolved during the first heating remains upon cooling, and the peak position continuously shifts toward the higher 2θ. The corresponding decrease of the *d* spacing was found to be a linear function of temperature, as a result of a thermal shrinkage. The coefficient of thermal expansion (CTE) of P-Ct deduced from the cooling WAXD patterns in Figure 4b is approximately 3.4×10^{-4} nm/°C, which is on the same order of magnitude as those reported for PMPCS.[15]

The phase behavior of P-Ct as shown in Figure 4 is highly reminiscent of that of the MJLCPs with Φ phases. The strong diffraction at low angle is the signature of the molecular rods of P-Ct. Parts a and b ofFigure 5 are the 2D WAXD patterns of the oriented P-Ct sample at room temperature, with the X-ray incident beam perpendicular and parallel to the shear direction, respectively. The sample was first sheared at 320 °C and then annealed at 240 °C for 12 h under nitrogen. In Figure 5a, only the higher-angle amorphous scattering is observed to be more or less concentrated on the meridian (the fiber direction), which

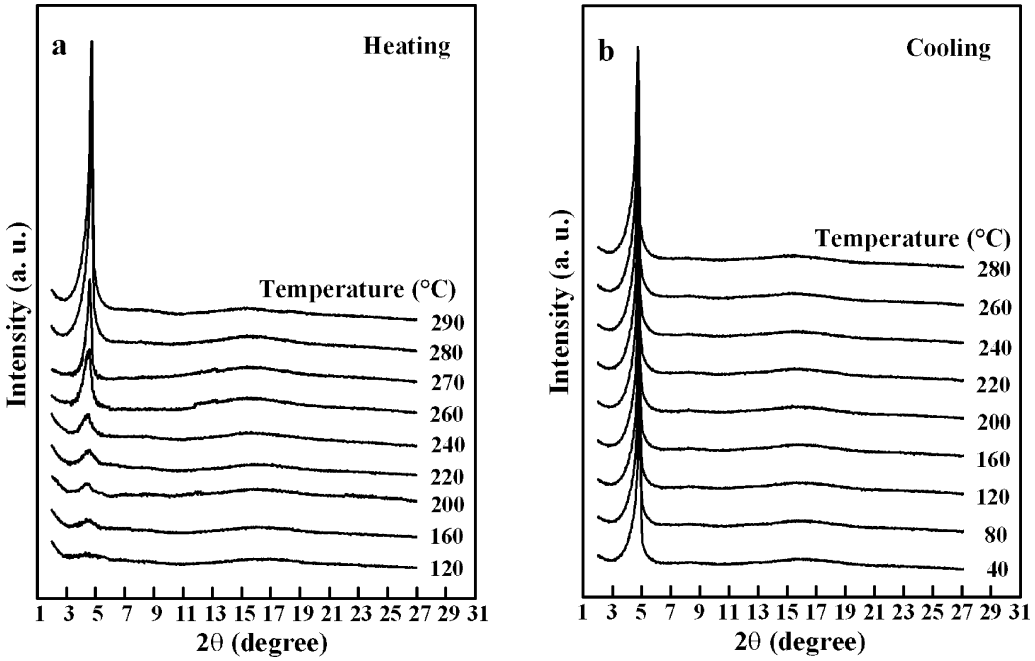

Figure 4. Two sets of 1D WAXD patterns of P-Ct obtained during the first heating (a) and the subsequent cooling (b).

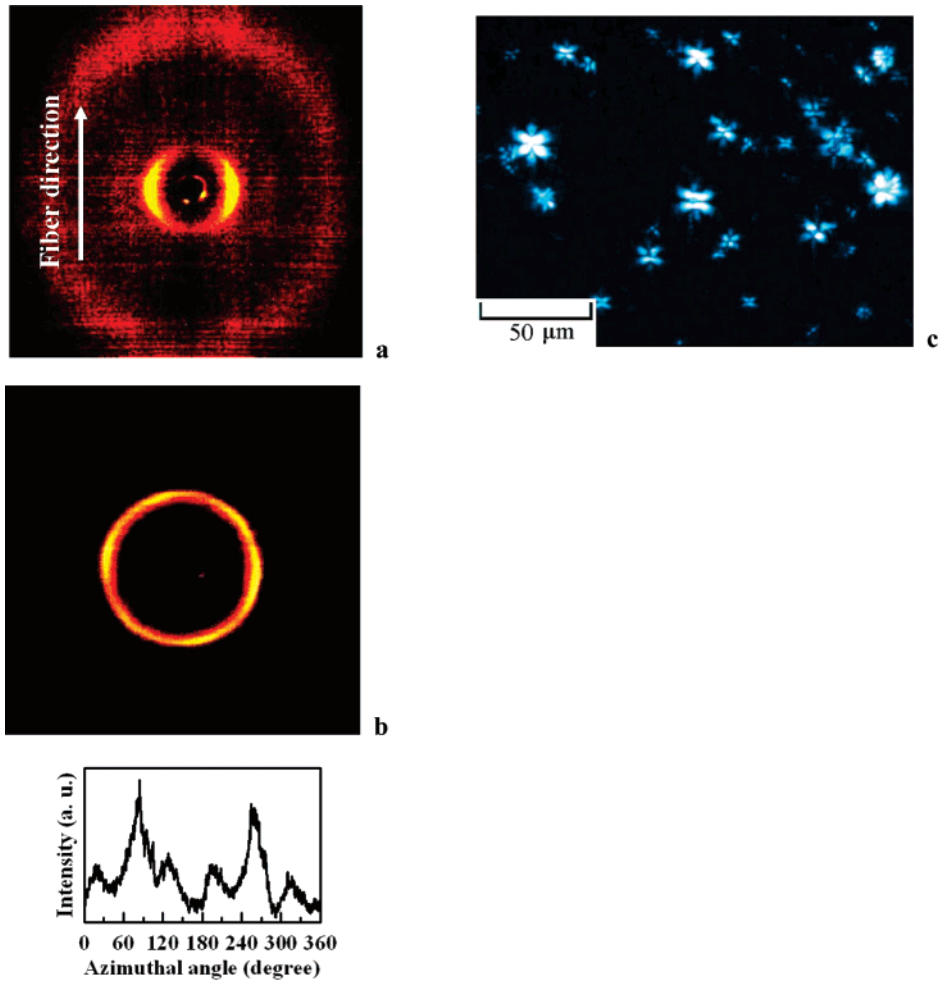

Figure 5. (a and b) 2D WAXD fiber patterns of P-Ct recorded at room temperature. The X-ray incident beam is perpendicular (a) and parallel (b) to the fiber axis. The lower part of part b is the azimuthal scanning data of the diffraction at 2θ of 4.73° of P-Ct. (c) PLM image of P-Ct at 280 °C.

shall be ascribed to the disorder along the chain direction. On the other hand, a pair of strong diffraction arcs is shown on the equator at the 2θ of 4.73° (i.e., d spacing of 1.85 nm), indicating an order along the direction perpendicular to the fiber axis. This low-angle diffraction presents six arcs when the incident beam is aligned parallel to the fiber direction as shown in Figure 5b.

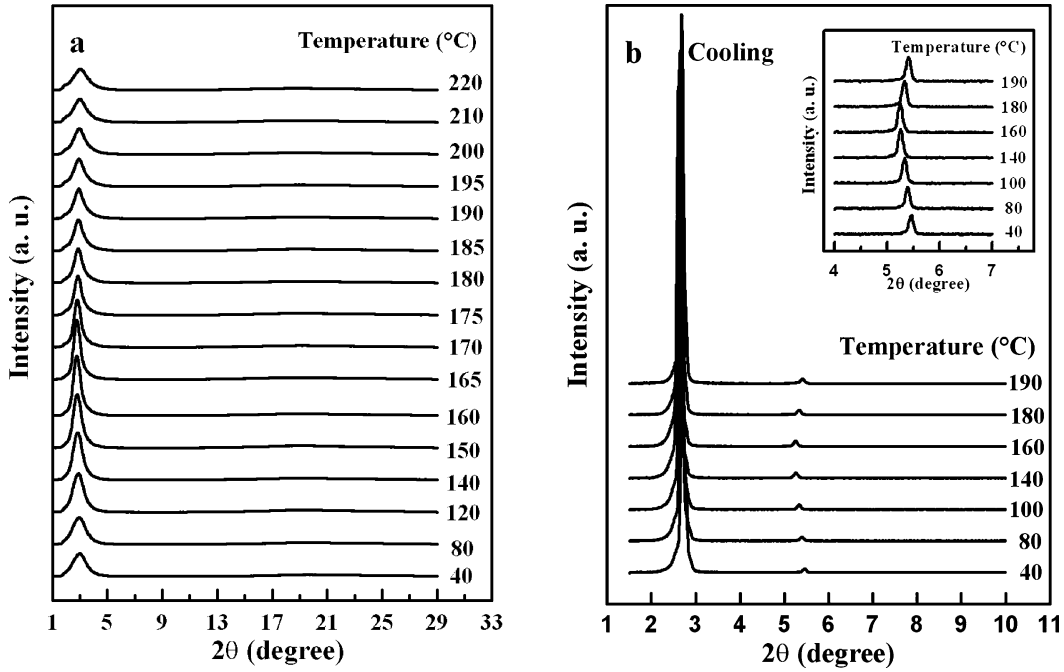

Figure 6. Two sets of 1D WAXD patterns of P-OC10 obtained during the first heating (a) and the cooling (b). The inset of part b is the enlarged patterns of the second-order diffraction.

The corresponding azimuthal intensity profile shows 60° between the two adjacent diffraction maxima (see the lower part of Figure 5b), of which the uneven intensities shall be due to the imperfection of the chain orientation. This confirms a hexagonal lateral packing of the rods with an average molecular rod diameter of 2.16 nm. Since the higher order diffractions are missing, a Φ_{HN} phase may be assigned for P-Ct. This assignment can be supported by our PLM result. As shown in Figure 5c, a star-shaped texture is observed for the P-Ct at 280 °C, which is a characteristic of Φ phases.[15] Note that the P-Ct rod diameter of 2.16 nm in the Φ_{HN} phase is just slightly larger than the calculated length of the side group (2.10 nm). Therefore, the fully rigid side groups of P-Ct are almost perpendicular to the rod long axis within the column. The Φ_{HN} phase of P-Ct was stable up to the temperature of thermal degradation.

While the P-Ct exhibits the typical Φ_{HN} phase of MJLCP, the WAXD experiments of the P-OC*m* suggested that such an MJLCP can form stable smectic LC phases. We use the P-OC10 as an example, and its 1D WAXD experimental results are presented in Figure 6. The as-cast amorphous sample demonstrates a scattering halo at a low 2θ angle of 2−4° at low temperature. Upon the first heating (see Figure 6a, recorded using Bruker D8Discover), a diffraction peak rapidly develops at a 2θ of ∼2.8° after the sample enters its glass transition region. Further heating leads to the peak slightly shifting to a lower angle, which may be mainly due to thermal expansion. However, the peak decreases in intensity and moves in the opposite direction when the temperature exceeds 165 °C, which corresponds to the onset of the broad endothermic process observed on the DSC heating curve. After 190 °C where the major endotherm starts, the diffraction peak further shifts to a higher angle accompanied with a more obvious peak broadening. Above 205 °C, a scattering halo appears, indicating that the sample becomes isotropic.

The diffraction is restored and can be retained below the T_g of the sample upon cooling. Figure 6b presents a set of 1D WAXD patterns of P-OC10 recorded using Philips X'pert Pro during cooling below 200 °C. As more sample amounts and longer exposure times were used, the diffraction intensity looks stronger compared with that shown in Figure 6a. Of particular interest is that a second-order diffraction at 2θ of ∼5.6° can be unambiguously recognized in the patterns (also see the inset of Figure 6b). The scattering vector ratio of the two diffractions follows 1:2 at each temperature, indicating a smectic structure of the sample. Moreover, since the layer period measured from the diffraction is almost identical to the side-chain length, we may assign the S_A phase for P-OC10. For all four of the P-OC*m*s, the 1D WAXD experiments led to the same conclusion.

The S_A structure of P-OC*m*s was further confirmed via 2D WAXD experiments. To avoid thermal degradation, the P-OC*m*s samples were mechanically sheared between 170 and 180 °C, rather than in the isotropic state. Figure 7a shows the 2D WAXD patterns of the oriented P-OC8 sample recorded at room temperature with the X-ray incident beam perpendicular to the shear direction. The meridian (fiber axis) and equator of the 2D pattern are indexed by the solid and dashed line, respectively. The integral intensities along the meridian and equator are shown in Figure 7b. On the equator, a very strong diffraction pair with a *d* spacing of 2.87 nm is observed. Moreover, although its intensity is much lower, a second-order diffraction on the equator can be clearly seen, of which the scattering vector ratio to the first one is 2:1. In the high 2θ region, the scattering halo is more or less concentrated on the meridian. As shown in Figure 7b, the halo possess two intensity maximums, which are located at a 2θ of around 21° and 25° (*d* spacings of 0.42 and 0.35 nm), respectively. As the polymer backbones shall be oriented along the shear direction, the halo at 21° with a *d* spacing of ∼0.42 nm can be correlated with the projection of two repeating units along the chain axis.[15] The halo at 25° may be possibly attributed to the width of the mesogens, which indicates that the mesogen directors are nearly perpendicular to the shear direction. Such a 2D WAXD pattern evidences a typical S_A phase.

Figure 8 summarizes the *d* spacings of the low angle diffraction/scattering of P-OC*m*s as a function of temperature deduced from the first heating 1D WAXD experiments after the S_A structures of P-OC*m*s appeared at 140 °C. When the S_A

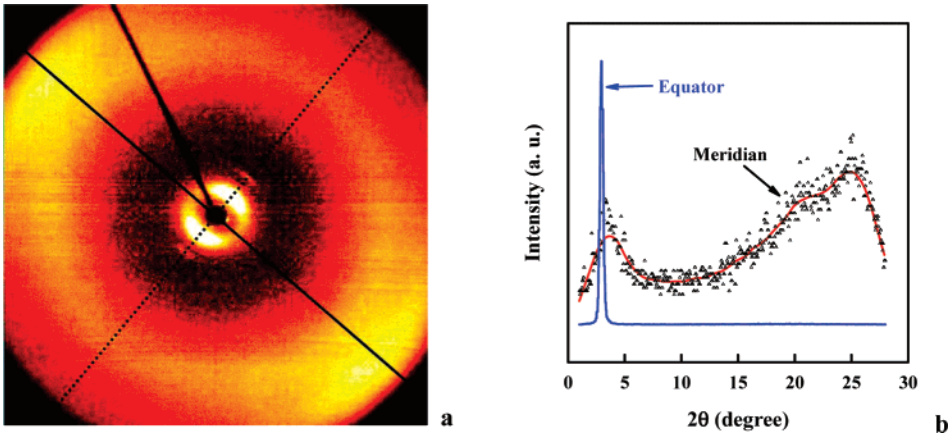

Figure 7. (a) 2D WAXD fiber pattern of P-OC8 recorded at room temperature. The meridian (fiber axis) and equator are indexed by the solid and dashed lines, respectively. The X-ray incident beam is perpendicular to the fiber axis. (b) Intensity profiles along the meridian and equator. Since the intensity along the meridian is low and scattered (see the symbol ▲), the red line represents the data after smoothing to illustrate more clearly the two scattering maximums in high-angle region.

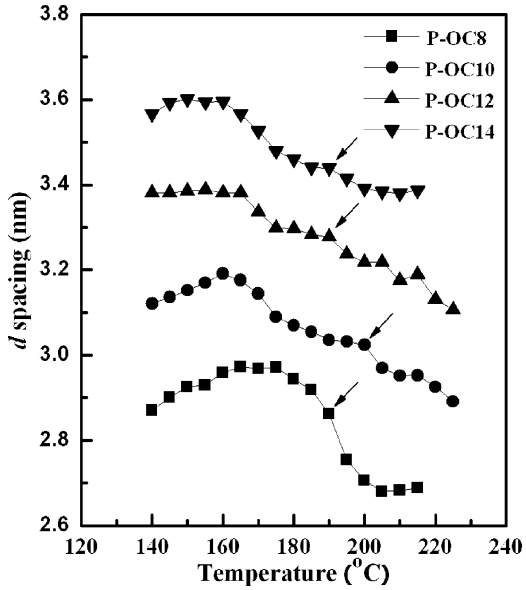

Figure 8. *d* spacings of the low-angle diffraction/scattering of P-OC*m*s as a function of temperature.

phases are well developed at around 160 °C, the *d* spacings reaches a plateau or maximum, which are almost identical to the calculated lengths of the side chains with the assumption that the *n*-alkoxy substituents are in an all-trans conformation. However, when entering the temperature range of the broad endothermic process as shown in Figure 3, the *d* spacings start to decrease, which may result from the *n*-alkoxy tails gradually losing the all-trans conformation and/or from the mesogens tilting with respect to the smectic layer normal. This will finally lead the S_A to transform into the N phase. As indexed by the arrows in Figure 8, a relatively large and sudden drop of the *d* spacing occurs at the temperature close to the end of the broad endotherm of the sample, indicating that the N phase forms. Afterward, the N-to-I transition will takes place.

We further used PLM heating and cooling experiments to illustrate the phase transitions. The PLM samples were sandwiched in between two cover glasses and, therefore, were protected from direct contact with the air. Parts a and b of Figure 9 demonstrate two PLM textures of P-OC10 obtained at 205 and 195 °C, respectively. After cooling from the isotropic state to 205 °C, a Schlieren texture with two and four brushes, a characteristic of an N phase, is observed. Further cooling to 195 °C leads to the disappearance of the two brushes. As indexed by the arrows in Figure 9, the original two brushes in Figure 9a merge to form the four brushes, indicating an N-to-S_A transition. The reverse texture evolution was observed upon heating. Combining the experimental results from different methods, we propose that the transition of the four P-OC*m*s follow the sequence of $S_A \leftrightarrow N \leftrightarrow I$.

Compared with those incorporated in the MJLCPs we synthesized before,[5−11,15−18] the side chains based on the oxadiazole group possess more rigid and a straight mesogen core with stronger interaction, particularly the $\pi-\pi$ interaction. In this context, the parallel packing of the mesogens shall be favored. For the polymers we studied here, comparison between the P-Ct and the P-OC*m*s gives that the only difference in chemical structure is the substituents on the side chains. However, they exhibit completely different LC structures. Our experimental results suggest that LC phase structures of the polymers are dependent not only on the mesogen−mesogen interaction but also on the balance between this interaction and steric hindrance. Figure 10 depicts a schematic drawing of the molecular packing of P-Ct in the Φ_{HN} phase and P-OC*m*s in the S_A phase. We conclude from the WAXD results that both P-Ct and P-OC*m* have their mesogenic side groups preferentially perpendicular to the chain axis. In the Φ_{HN} phase of P-Ct, the polymer chains form molecular rods as the LC building blocks. When viewed from the rod axis, i.e., the chain axis, the P-Ct's side chains might have an overall random distribution of the mesogen directors. We consider that for P-Ct with fully rigid side chains, the steric hindrance imposed on the polymer backbone still dominates the chain packing. However, while relatively long flexible tails are introduced, the mobility of the side chains of P-OC*m*s will be greatly enhanced. In this case, the parallel packing of the side chains is realized so that the interaction between mesogen cores can be maximized, resulting in the S_A phase of P-OC*m*s. As the P-OC*m*'s side chains are laterally jacketed to the polyethylene backbone through a single carbon−carbon bond, a "microphase separation" between the backbones and the side chains,[54] which is commonly observed in side-chain LC polymers with reasonably long flexible spacers, is unlikely to occur when the P-OC*m*s molecules pack in the S_A phase. For an individual P-OC*m* molecule, the backbone may be squeezed between two adjacent layers of the mesogens, making the whole molecule ribbonlike. As mentioned above, the T_g of the four P-OC*m*s is almost independent of the alkoxy tail length. We presume that the alkoxy tails improve the side-chain mobility and thus facilitate the parallel packing of the

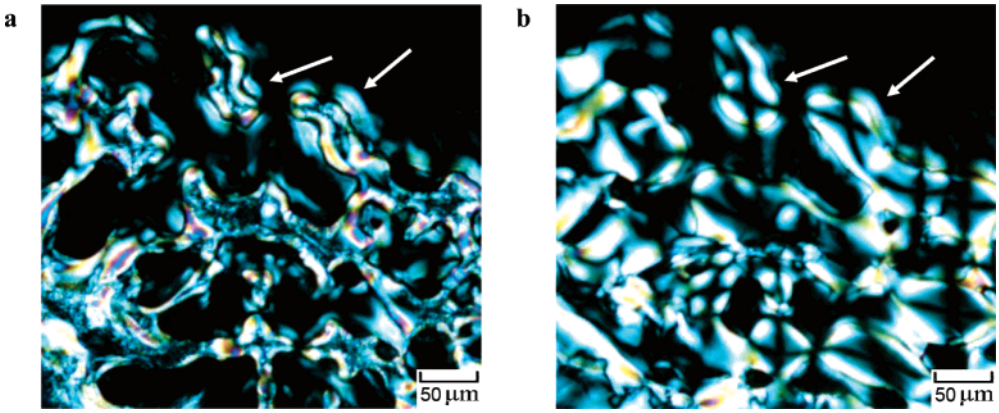

Figure 9. PLM images of P-OC10 taken from the same sample at (a) 205 °C and (b) 195 °C. As indexed by the arrows, the two brushes in part a disappear and the four brushes appear in part b after cooling to 195 °C.

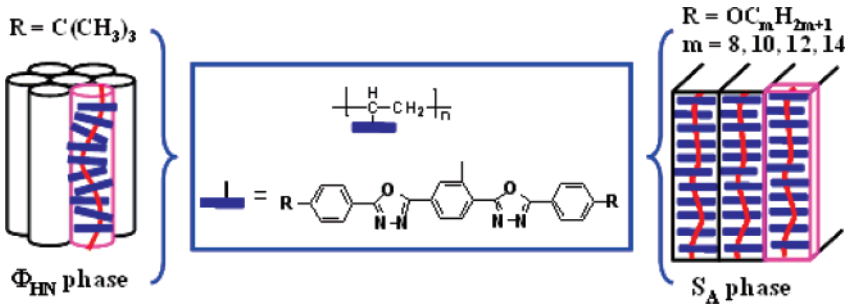

Figure 10. Schematic drawing of the LC phase structures of the polymers. P-Ct (R = $C(CH_3)_3$ forms the Φ_{HN} phase; P-OC*m* (R = OC_mH_{2m+1}, *m* = 8, 10, 12, 14) forms the S_A phase.

mesogens in the S_A phase. Once the ribbonlike molecular structure is formed, the alkoxy tail effect on the main chain relaxation might be screened. This could be the reason to account for the glass transition behavior we observed.

It is of interest to further examine the alkoxy length effect on the phase structure. We speculate that reducing the length of the alkoxy tails in the P-OC*m* will gradually decrease the side-chain mobility. Once the steric hindrance cannot be overcome, the P-OC*m* with short alkoxy tails shall pack into an Φ phase similar to that of the P-Ct. However, the monomers M-OC*m* ($m < 8$) were found to be difficultly dissolved in common organic solvents or be polymerized to a sufficiently high MW. The synthesis of the P-OC*m* ($m < 8$) is still currently underway in our laboratory.

Conclusion

We have successfully synthesized a series of vinyl monomers (M-Ct and M-OC*m*) containing the electron-deficient functional group of 1,3,4-oxadiazole. Upon using conventional radical polymerization, we further obtained the mesogen-jacketed liquid crystalline polymers of P-Ct and P-OC*m*. The chemical structures of the monomers and polymers were confirmed by various characterization techniques. Their phase structures and transitions of the polymers were investigated. Compared with the T_g of 223 °C for P-Ct with fully rigid side chains, the T_g's of P-OC*m*s with flexible alkoxy tails are nearly 70 °C lower. This indicates that the flexible alkoxy tails in P-OC*m*s greatly enhance the molecular mobility. The P-Ct formed the Φ_{HN} phase that is typical for MJLCPs, wherein the building blocks of the LC phase were the molecular rods of P-Ct. However, with the relatively long flexible tails at both ends of the mesogen, the four P-OC*m*s obtained sufficiently high side-chain mobility to overcome the steric hindrance. In this case, the mesogen interaction leads the sample to form well-defined smectic A (S_A) phases at low temperature. The transition of the four P-OC*m*s follows the sequence of $S_A \leftrightarrow N \leftrightarrow I$. As the side chain is laterally jacketed to the polyethylene backbone through a single carbon−carbon bond, the parallel packing of the mesogenic groups of the P-OC*m*s in the S_A phase makes the molecules somewhat ribbonlike. The comparison between P-Ct and P-OC*m*s indicates that the flexibility of the side-chain tails is crucial to determine the LC structures. Therefore, this research demonstrates that simply changing the chemical structures of a small portion of the MJLCP may greatly vary the molecular packing behavior and thus the molecular shape in LC phase structures.

Acknowledgment. This research was supported by the National Natural Science Foundation of China (Grant Numbers 20634010, 20574002, 20025414, and 20234020) and the Key Project of Chinese Ministry of Education (Grant Number 104005).

Supporting Information Available: Characterization results of mass spectrometry and elementary analysis of the monomers and IR and ^1H NMR of the polymers. This material is available free of charge via the Internet at http://pubs.acs.org.

References and Notes

(1) Donald, A. M.; Windle, A. H. *Liquid Crystalline Polymers*; Cambridge University Press: Cambridge, U.K., 1992.
(2) McArdle, C. B. *Side-Chain Liquid Crystal Polymer*; Blackie: Glasgow, Scotland, 1989.
(3) Finkelmann, H.; Happ, M.; Portugall, M.; Ringsdorf, H. *Macromol. Chem.* **1978**, *179*, 2541.
(4) Hessel, F.; Finkelmann, H. *Polym. Bull.* **1985**, *14*, 375.
(5) Zhou, Q. F.; Li, H. M.; Feng, X. D. *Macromolecules* **1987**, *20*, 233.
(6) Zhou, Q. F.; Zhu, X. L.; Wen, Z. Q. *Macromolecules* **1989**, *22*, 491.
(7) Pragliola, S.; Ober, C. K.; Mather, P. T.; Leon, H. G. *Macromol. Chem. Phys.* **1999**, *200*, 2338.
(8) Zhang, D.; Zhou, Q. F.; Ma, Y. G.; Wan, X. H.; Feng, X. D. *Polym. Adv. Technol.* **1997**, *8* (4), 227.

(9) Zhang, D.; Liu, Y. X.; Wan, X. H.; Zhou, Q. F. *Macromolecules* **1999**, *32*, 5183.
(10) Yu, Z. N.; Wan, X. H.; Zhang, H. L.; Chen, X. F.; Zhou, Q. F. *Chem. Commun.* **2003**, 974.
(11) Chen, X. F.; Tenneti, K. K.; Li, C. Y.; Bai, Y. W.; Zhou, R.; Wan, X. H.; Fan, X. H.; Zhou, Q. F. *Macromolecules* **2006**, *39*, 517.
(12) Hardouin, F.; Mery, S.; Achard, M. F.; Noirez, L.; Keller, P. *J. Phys. II* **1991**, *1*, 511. Hardouin, F.; Mery, S.; Achard, M. F.; Noirez, L.; Keller, P. *J. Phys. II* **1991**, 871 (erratum).
(13) Hardouin, F.; Leroux, N.; Mery, S.; Noirez, L. *J. Phys. II* **1992**, *2*, 271.
(14) Wan, X. H.; Zhang, F.; Wu, P.; Zhang, D.; Feng, X. D.; Zhou, Q. F. *Macromol. Symp.* **1995**, *96*, 207.
(15) Ye, C.; Zhang, H. L.; Huang, Y.; Chen, E. Q.; Lu, Y. L.; Shen, D. Y.; Wan, X. H.; Shen, Z. H.; Cheng, S. Z. D.; Zhou, Q. F. *Macromolecules* **2004**, *37*, 7188.
(16) Zhao, Y. F.; Fan, X. H.; Wan, X. H.; Chen, X. F.; Yi, Y.; Wang, L. S.; Dong, X.; Zhou, Q. F. *Macromolecules* **2006**, *39*, 948.
(17) Tang, H.; Zhu, Z. G.; Wan, X. H.; Chen, X. F.; Zhou, Q. F. *Macromolecules* **2006**, *39*, 6887.
(18) Zhang, H. L.; Yu, Z. N.; Wan, X. H; Zhou, Q. F.; Woo, E. M. *Polymer* **2002**, *43*, 2357.
(19) Tu, H. L.; Wan, X. H.; Liu, Y. X.; Chen, X. F.; Zhang, D.; Zhou, Q. F.; Shen, Z. H.; Ge, J. J.; Jin, S.; Cheng, S. Z. D. *Macromolecules* **2000**, *33*, 6315.
(20) Yin, X. Y.; Ye, C.; Ma, X.; Chen, E. Q.; Qi, X. Y.; Duan, X. F.; Wan, X. H.; Cheng, S. Z. D.; Zhou, Q. F. *J. Am. Chem. Soc.* **2003**, *125*, 6854.
(21) Percec, V.; Heck, J.; Tomazos, D.; Falkenberg, F.; Blackwell, H.; Ungar, G. *J. Chem. Soc., Perkin Trans. 1* **1993**, 2799.
(22) Percec, V.; Ahn, C. H.; Barboiu, B. *J. Am. Chem. Soc.* **1997**, *119*, 12978.
(23) Forster, S.; Neubert, I.; Schluter, A. D.; Linder, P. *Macromolecules* **1999**, *32*, 4043.
(24) Ungar, G. *Polymer* **1993**, *34*, 2050.
(25) Allegra, G.; Meille, S. V. *Macromolecules* **2004**, *37*, 3487.
(26) Tu, Y. F.; Wan, X. H.; Zhang, D.; Zhou, Q. F.; Wu, C. *J. Am. Chem. Soc.* **2000**, *122*, 10201.
(27) Gopalan, P.; Zhang, Y. M.; Li, X. F.; Wiesner, U.; Ober, C. K. *Macromolecules* **2003**, *36*, 357.
(28) Zhang, H. L.; Chen, X. F.; Wan, X. H.; Zhou, Q. F.; Woo, E. M. *Polym. Int.* **2003**, *52*, 92.
(29) Yi, Y.; Fan, X. H.; Wan, X. H.; Li, L.; Zhao, N.; Chen, X. F.; Xu, J.; Zhou, Q. F. *Macromolecules* **2004**, *37*, 7610.
(30) Zhang, J.; Yu, Z. N.; Wan, X. H.; Chen, X. F.; Zhou, Q. F. *Macromol. Rapid Commun.* **2005**, *26*, 1241.
(31) Li, C. Y.; Tenneti, K. K.; Zhang, D.; Zhang, H.; Wan, X.; Chen, E. Q.; Zhou, Q. F.; Carlos, A.-O.; Igos, S.; Hsiao, B. S. *Macromolecules* **2004**, *37*, 2854.
(32) Tenneti, K. K.; Chen, X. F.; Li, C. Y.; Tu, Y. F.; Wan, X. H.; Zhou, Q. F.; Sics, I.; Hsiao, B. S. *J. Am. Chem. Soc.* **2005**, *127*, 15481.
(33) Komp, A.; Finkelmann, H. *Macromol. Rapid Commun.* **2007**, *28*, 55.
(34) Lecommandoux, S.; Noirez, L.; Achard, M. F.; Hardouin, F. *Macromolecules* **2000**, *33*, 67.
(35) Lecommandoux, S.; Hardouin, F.; Dianoux, X. J. *Eur. Phys. J. B* **1998**, *5*, 79.
(36) Arehart, S. V.; Pugh, C. *J. Am. Chem. Soc.* **1997**, *119*, 3027.
(37) Pugh, C.; Bae, J. Y.; Diharia, J.; Ge, J. J.; Cheng, S. Z. D. *Macromolecules* **1998**, *31*, 5188.
(38) Kim, G. H.; Pugh, C.; Cheng, S. Z. D. *Macromolecules* **2000**, *33*, 8983.
(39) Small, A. C.; Pugh, C. *Macromolecules* **2002**, *35*, 2105.
(40) Chen, S.; Gao, R.-C.; Zhao, X.-D.; Chen, X.-F.; Fan, X.-H.; Xie, P.-Y.; Zhou, Q.-F. *Macromolecules* **2007**, *40*, 5718.
(41) Adachi, C.; Tsutsui, T.; Saito, S. *Appl. Phys. Lett.* **1989**, *55*, 1489.
(42) Kraft, A.; Grimsdale, A. C.; Holmes, A. B. *Angew. Chem., Int. Ed.* **1998**, *37*, 402.
(43) Mitschke, U.; Bäuerle, P. *J. Mater. Chem.* **2000**, *10*, 1471.
(44) Hughes, G.; Bryce, M. R. *J. Mater. Chem.* **2005**, *15*, 94.
(45) Adachi, C.; Tokito, S.; Tsutsui, T.; Saito, S. *Jpn. J. Appl. Phys.* **1988**, *27*, L713.
(46) Wang, C.; Jung, G.-Y.; Batsanov, A. S.; Bryce, M. R.; Petty, M. C. *J. Mater. Chem.* **2002**, *12*, 173.
(47) Chien, Y.-Y.; Wong, K.-T.; Chou, P.-T.; Cheng, Y.-M. *Chem. Commun.* **2002**, 2874.
(48) Cha, S. W.; Choi, S.-H.; Kim, K.; Jin, J.-I. *J. Mater. Chem.* **2003**, *13*, 1900.
(49) Peng, Z.; Bao, Z.; Galvin, M. E. *Chem. Mater.* **1998**, *10*, 2086.
(50) Chen, Z.-K.; Meng, H.; Lai, Y.-H.; Huang, W. *Macromolecules* **1999**, *32*, 4351.
(51) Wang, C.; Kilitziraki, M.; Palsson, L.-O.; Bryce, M. R.; Monkman, A. P.; Samuel, I. D. W. *Adv. Funct. Mater.* **2001**, *11*, 47.
(52) Stollé, R. *Ber. Dtsch. Chem. Ges.* **1899**, *32*, 797.
(53) Stollé, R.; Hille, R. J. *Prakt. Chem.* **1904**, *69*, 481.
(54) Davidson, P. *Prog. Polym. Sci.* **1996**, *21*, 893.

MA071670T